Micro-SORS, diffusion processes and heritage science: a non-destructive and systematic investigation

A.Botteon[a,b*], M.Realini[a] , C.Colombo[a], C.Conti[a*], P.Matousek[c] and C.Castiglioni[b]

[a] *Consiglio Nazionale delle Ricerche, Istituto di Scienze del Patrimonio Culturale (ISPC), Via Cozzi 53, 20125, Milano, Italy.*

[b] *Politecnico di Milano, Department of Chemistry, Materials and Chemical Engineering "G. Natta", piazza Leonardo da Vinci 32, 20131 Milano, Italy.*

[c] *Central Laser Facility, Research Complex at Harwell, STFC Rutherford Appleton Laboratory, UK Research and Innovation (UKRI), Harwell Oxford, OX11 0QX, United Kingdom.*

* Corresponding authors: alessandra.botteon@polimi.it, claudia.conti@cnr.it

Key words: Micro-spatially offset Raman spectroscopy, diffusion, penetration depth, non-destructive, Cultural Heritage, Heritage Science

ABSTRACT

In this paper, a systematic investigation is carried out to test micro-SORS capability of non-destructively characterise a system where an agent diffuses into a turbid matrix with potential applications in Heritage Science and elsewhere. Defocusing micro-SORS experiments were performed on two specially designed sample sets with controlled characteristics. Three parameters have been considered, namely penetration depth, concentration of the agent and its profile within the matrix. A relative agent/matrix Raman intensity decay rate is observed when the microscope objective is moved away from the sample surface, and the slope of this ratio trend was found to correlate with the penetration depth of the agent involved in the diffusion process. In situations where the concentration profile is known, the penetration depth of the agent can be predicted using the slope of the normalized agent/matrix Raman intensity decay rate. This outcome opens new perspective for non-destructively monitoring the efficacy of conservation treatments, basing on the penetration depth of the products as well as provides an analytical tool for other applications where the penetration of an agent into a diffusely scattering matrix is involved such as drug perfusion through skin, pharmaceutical tablet dissolution process and numerous others.

1. INTRODUCTION

When an agent diffuses into a solid matrix, it is absorbed up to a certain depth defined as a certain fraction of the initial concentration of the agent at the surface of the matrix and distributed inside the matrix following a certain time-dependent concentration profile. The absorption process can either involve a reaction between the agent and the matrix or being non-reactive [1].

Agent penetration depth and concentration profile are important factors for the characterization of an agent-matrix system. The study of diffusion proprieties is relevant in several fields, including semiconductors industry, where, for instance, the diffusion of fluorinated PMMA trough a non-fluorinated PMMA layer at the semiconductor/dielectric interface is controlled for improving the performance of the organic field-effect transistors [2]. In biomedical field, the study of diffusion proprieties is relevant for monitoring the absorption of drugs in tissues [3,4], whereas in heritage science, it is essential for evaluating the performance of a treatment [5–9], for accessing the distribution of decay products and degradation agents in matrix [10,11] or for monitoring the absorption of solvents used for cleaning [12]. In several abovementioned situations, it is particularly important to observe the diffusion process at the micro-scale, since in several situations consolidants, fixatives, decay products and solvent diffuse to within a millimetre depth. To date the most common protocol for obtaining this type of information involves destructive procedures such as the stratigraphical analysis of samples in cross-section [5,7–10,13–15]. However in a number of areas, including Cultural Heritage, the items may have a high intrinsic value or cannot be perturbed for other functional reasons and non-destructive approaches are much more preferable. Moreover, the analysis of cross-sections may suffer from an inadequate statistical sampling as the information obtained is limited to a specific sampling area. A number of non-destructive methods have been proposed for studying diffusion processes in Cultural Heritage; these include neutron imaging and tomography [5,6,16] and X-ray micro-computed tomography [17], although these are limited by the scarce accessibility and may lack of molecular specificity. Recently, micro-Spatially Offset Raman Spectroscopy (micro-SORS), a highly chemical specific and ready to use method, has been proposed for studying diffusion processes in heritage science-related situations [18]. Micro-SORS is a non-destructive technique able to retrieve the molecular composition of the inner portions of turbid materials (at the micro-scale) directly from their surface. Micro-SORS combines SORS and microscopy, and is mainly used to access the composition of micro-layer sequences in stratified materials [19–21]. Recently, through a basic proof of concept study we demonstrated the basic capability of micro-SORS to track an agent penetrating into a turbid matrix, where no distinct layers are otherwise present [18]: defocusing micro-SORS [22,23], the most basic variant of micro-SORS, was used to study mock-up samples where a gypsum matrix was impregnated with two products used in conservation yard. The studied samples possessed different penetration depths of the products, and it was possible to discriminate these by considering the difference of their relative agent-matrix Raman intensity ratio decay rate as a function of SORS displacement.

Here, a more extensive study is presented with the intention to take a step forward on the study of diffusion processes, considering other parameters that could potentially contribute to the modification of the intensity ratio decay rate. In real situations, several factors can affect the diffusion proprieties; for instance, a non-homogeneous degradation of the matrix can produce a non-homogeneous penetration of a product. Nonetheless, to investigate of the micro-SORS capability and limitations, at this stage, it is necessary to build a model that simplify what can be encountered in a conservation yard. To do that, here no decay process affecting the materials were took into consideration, and three variables have been selected as the most significant for the description of the diffusion processes: i) the penetration depth of the agent ii) the absolute concentration of the product applied at the surface of matrix, and iii) the function, *C(x),* with which this concentration decreases within the inner portion of the material (namely, the concentration profile). It is shown that it is crucial to know the shape of concentration profile in the matrix (not necessarily its characteristic depth) for micro-SORS to be able to provide information about the penetration depth of a product, thus enabling it to evaluate real case situations. However often the shape of concentration profile can be assumed from the way matrix and agent interact and the way the agent is applied at the surface. For example, for non steady-state diffusion in constant dose conditions, when the diffusant is initially concentrated in a very thin layer (*e.g.* agent applied thinly with a brush), a half-Gaussian solution of the diffusion equation applies:

$$C(x,t) = \frac{M}{\sqrt{\pi Dt}} \exp\left(-\frac{x^2}{4Dt}\right)$$

where *C (x,t)* is the concentration field, x is the depth, *M* is number of diffusing particles per unit area, *D* is the diffusion coefficient of the considered species and *t* time of diffusion, with $2\sqrt{Dt}$ as characteristic diffusion length [24]. In a constant source condition (*e.g.* a very large amount of agent applied on top of matrix which remains present throughout the diffusion process), the solution of the diffusion equation is an error function (*erf*) [24,25]. In this case, concentration field *C (x, t)* may be expressed as:

$$C(x,t) = C_s \operatorname{erfc}\left(\frac{x}{2\sqrt{Dt}}\right)$$

Where C_s is the fixed concentration the matrix is exposed to and *erfc* is denoted as *complementary error function:*

$$\operatorname{erfc}(z) \equiv 1 - \operatorname{erf}(z)$$

with $2\sqrt{Dt}$ being characteristic diffusion depth [24]. This can often present a good approximation of such systems, although real case situations may not be ideal stable and homogeneous systems, and more sophisticated mathematical models may be required to describe the diffusion process in detail in more complex scenarious [26].

It is worth mentioning that, in a number of situations, the diffusion process ends due to *e.g.* solvent evaporation, diffusant hardening (*e.g.* polymerization) or reagent depletion, and the concentration profile then remains unchanged. In this study, two sample sets were prepared mimicking a situation where the diffusion process is not any longer in progress, and the penetration depth of the agent is fixed in time. In this way, there was no need of including the temporal variable in the data treatment.

The two sample sets have a varying degree of complexity: the first set consists of a simplification of a diffusion system that allows to easily comprehend what the role of the considered variables is. It crudely simulates a paint application on a paper substrate (watercolour), and in a wider perspective, it approximates a liquid diffusion into an absorbing substrate, without the occurrence of an accompanying chemical reaction; for instance, when a solvent is used to remove a specific compound present on an object surface, but it diffuses also in the underlying substrate without interacting with it.

The second samples set was prepared with the aim to loosely imitate a common, realistic situation encountered in conservation yard and is of a more complex nature. It comprises a carbonatic stone treated with ammonium oxalate, where the diffusion process involves also a chemical reaction. The reaction of ammonium oxalate and calcium carbonate leads to the formation of calcium oxalate (whewellite, $CaC_2O_4 \cdot H_2O$ and weddellite, $CaC_2O_4 \cdot 2H_2O$), a low solubility compound able to restore the stone or plaster network preventing the loss of the superficial material [27]. The penetration depth of the newly formed calcium oxalate cannot be known a priori as it depends on several factors including the substrate porosity and its decay, eventual aggregate size and distribution and the concentration of the solution, to name a few. To date, the determination of calcium oxalate penetration depth was carried out destructively on the cross-sections of treated plasters and stones using subsequent Raman microscopy [7–9,28]. Moreover, neutron tomography was used to study the distribution and penetration depth of calcium oxalate in a carbonatic stone (Noto stone) [5]. Similarly, neutron imaging was used to measure the diffusion coefficient of a carbonatic stone treated with ammonium oxalate and the concentration of newly formed calcium oxalate [6]. As mentioned above, despite neutron imaging being a non-destructive approach it lacks of information on the molecular composition of the material and it is not an easily accessible tools, and not applicable in the field. Conversely, defocusing micro-SORS measurement can be performed with a conventional micro-Raman, without any software not hardware modification, with potential for in field deployment.

To understand technique fundamental characteristic in these scenarios and to have an easy to control of the desired characteristics of the samples (*e.g.* agent penetration depth) the samples were artificially assembled by stacking individual micro-layers on top of each other. Although this did not provide proper diffusion concentration gradients [24] it offers a good representation of these enabling, in particular, to

better understand how the SORS technique responds in different scenarios and ascertain with better clarity the technique fundamental capabilities as well as limitations. In all the measurements an assumption is made that that the matrix and agent light absorption is negligible at the laser and Raman wavelengths on the scale of photon propagation pathways [29], ie not impeding the photon migration process, which is a reasonable assumption at the concerned spectral range and microscopic scale of sample interactions in many practical scenarios.

2. MATERIAL AND METHODS

In samples set 1, paper was chosen as matrix, and a blue pigment (phthalocyanine blue, PB15) was used as penetrating agent. The pigment source was an acrylic blue paint purchased from Maimeri. The sheets of paper (each paper sheet is 90 µm thick) were imbibed with a paint suspension at two different starting concentrations aiming for obtaining a layer where the Raman signal of both the agent and the matrix were well visible to facilitate their unhindered monitoring. At the same time, the two concentrations were used to present a significant mutual difference in terms of Raman intensity of the pigment and that of the matrix. The more concentrated suspension provides a B/P (phthalocyanine blue/paper) intensity ratio of approximately 15.5 and the less concentrated suspension of about 6. The ratios were calculated using the intensities of the 1530 cm^{-1} band of phthalocyanine blue and that of the 1377 cm^{-1} Raman band of paper.

The samples set was prepared by superimposing one or two coloured paper sheets with different combinations on top of several uncoloured paper sheets to build samples having different concentrations profiles and penetration depths (see Fig. 1). Samples 1A-1D were purposely assembled to exhibit a concentration profile where the concentration of the pigment remains constant up to a certain depth (concentration profile type 1). Conversely, sample 1E possess a concentration profile where the top and second layers have different concentrations of the blue pigment (concentration profile type 2). The uncoloured paper sheets that were used in all the samples serve to create an “infinite” matrix (> 4 mm) not to impede photon migration in z direction.

Samples set 2 mimics a carbonatic stone treated with ammonium oxalate; here we again used discrete layers for ease of control of sample properties but used two or three top layers of differing initial agent concentrations, which is more consistent with a real situation where a concentration profile is established with depth and across it. This set consists of four samples (samples 2A, 2B, 2C and 2D, Fig. 2) having layers of decreasing whewellite/calcite relative concentration from the top to the substrate. This change of relative concentration is consistent with a real, ammonium oxalate treatment, where calcium carbonate, the main constituent of carbonatic stones, is partially replaced by calcium oxalate after the reaction with ammonium oxalate. Whewellite, the more stable form of calcium oxalate was chosen over weddellite

because it is more commonly formed after the treatments. The mixture was prepared adding a finely ground whewellite powder purchased from Sigma and Aldrich to an industrial paint mixture purchased from Akzonobel, containing calcite and an acrylic resin. The samples were prepared applying the mixture over a calcium carbonate substrate, varying the number of layers or their thickness to simulate different penetration depths of the product, as well as changing the quantity of the calcite and whewellite in the layers to simulate different concentration profiles. The thickness of the layers, reported in figure 2, were measured using cross-sections. The W/C value indicated in Fig. 2 refers to the whewellite/calcite intensity ratio, calculated from the Raman spectra acquired on cross-sections. This ratio was calculated using the intensity of the 1462 cm^{-1} Raman band of whewellite and the 1087 cm^{-1} band of calcite. Indeed, the intensity ratio is proportional to the relative concertation of the two substances.

The two samples sets were prepared with the aim of mimicking a situation where the diffusion is fixed in time, which is consistent with several real case situations. This permits not to take into account a temporal variable in the data treatment. In fact, if the diffusion process is still ongoing (*e.g.* the diffusion of a viscous solvent that does not harden with time) this has to be taken into account while acquiring and interpreting the micro-SORS data, depending on the temporal scale the diffusion is progressing on.

The experiments were carried out using Horiba Jobin Yvon LabRAM HR800 Raman spectrometer equipped with a Peltier cooled CCD detector (1024 x 128 pixels) and coupled with an Olympus BX41 microscope. For all the measurements, 785 nm excitation laser and 20x microscope objective were used.

Preliminary conventional Raman measurements were carried out on the samples to check if the agent/matrix intensities fit the desired requirements, and the layers compositional homogeneity. These measurements were performed using a laser power of 100 mW, and an acquisition time ranging from 25 to 100s (5 to 10s, 5 to 10 co-additions) (spectra shown in Figs. 3 and 4).

With regards to the defocusing micro-SORS measurements, on each samples of the first set, 20 defocusing measurement series were performed, from imaged (in focus) position to 1000 µm defocusing distance (defocusing steps at 0, 100, 200, 300, 400, 600, 800 and 1000 µm). The spectra were collected with a laser excitation power of 100 mW and with an acquisition time of 25s (5s and 5 co-additions). The spectra of the 20 series were averaged, and the Raman intensity ratio trends were calculated using the height of a Raman band of phthalocyanine blue (1530 cm^{-1}) and a Raman band of paper matrix (1377 cm^{-1}).

On each sample of the second set, 10 defocusing series were performed, from imaged position to 1500 µm defocusing distance (defocusing step of 100 µm). The spectra were collected with an intensity of 100 mW and with an acquisition time of 100s (10s and 10 co-additions). The spectra of the 10 series were averaged,

and the Raman intensity ratio trends were calculated using the height of a Raman band of whewellite (1462 cm^{-1}) and of calcite (1087 cm^{-1}).

3. RESULTS AND DISCUSSION

3.1 Preliminary conventional Raman measurements

In Fig. 3 representative spectra collected on the surface of the coloured paper sheets are shown: both the Raman bands of the blue pigment (phthalocyanine blue, PB15) and those of the paper matrix are clearly visible.

To evaluate the homogeneity of the pigment distribution, several Raman spectra were collected on the front, on the back and in the cross-sections of the paper sheets. Local pigment/paper intensity fluctuations were found to be present, but the pigment was not preferentially accumulated on one of the two sides, nor along the depth of the cross-section. The relative standard deviation associated to 10, randomly selected spectra acquired on the paper sheets surface was 34 % for the more intense blue, and 45 % for the less intense blue. The local Raman intensity fluctuations are probably related to the matrix features: paper is composed by pressed fibres, that create preferential absorption of the pigment at the micro-scale. This inconvenience, quite common in real situations, was compensated during micro-SORS experiments by performing a high number (20) of series and averaging them, in line with a previous study focusing on appropriate micro-SORS methodologies for measuring heterogeneous materials [30].

In Fig. 4, representative conventional Raman spectra collected on the cross-sections of the second samples set are shown. In the spectra collected on the micro-layers, a Raman band of calcite (1087 cm^{-1}) and two peaks of whewellite (1462 and 1490 cm^{-1}) are visible, together with one band of the acrylic resin used as binder for the mixture (1003 cm^{-1}). The spectrum collected on the substrate exhibits the characteristic Raman band of calcite at 1087 cm^{-1}.

The W/C ratio were calculated from the average of 10 Raman spectra collected on each layer, using the intensity of 1492 cm^{-1} Raman band of whewellite and the 1087 cm^{-1} Raman band of calcite. The relative standard deviation associated to the ratio values was found to range from 7% to 20%. The present inhomogeneities were again dealt with using the averaging of multiple spectra (10) obtained from different sample locations.

3.2 Micro-SORS measurements

3.2.1 Samples set 1

In Fig. 5a the ratio plot of the samples having a concentration profile type 1 is shown (samples 1A-D). To make the trends comparable, a normalization was applied at 300 μm of defocusing to avoid the uncertainty of the first defocusing steps, that are more severely affected by the heterogeneity of the pigment distribution. The plot shows different ratio decay rates for the samples, and for a better understanding of the trends behaviour, a linear fitting was performed on the ratio curves (Fig. 5b)**.** From the linear fitting of the samples having concentration profile type 1 (samples 1A-1D) emerges that those with a single blue paper sheet (1A and 1B) have a faster ratio decay rate; on the contrary the samples with a higher penetration depth (1C and 1D) exhibit a ratio decay rate that decreases less rapidly. The slope of the decay curve correlating directly with the agent penetration depth is in line with was observed in our previous work concerning micro-SORS ability to track an agent penetrating into a turbid matrix [18]. In Fig. 6, the slopes (absolute values) obtained by the linear fitting are reported. With this data visualization, it is even more evident that the samples can be divided into two subgroups: the samples with a single blue paper sheet, showing a more steeply decrease, are grouped according to their higher slope absolute value (1A and 1B, group 1) and the samples with higher penetration depth have a smaller slope absolute value (group 2, samples 1C, 1D). Interestingly, the normalization procedure minimizes the effect produced by the different amount of pigment on both the surface and the subsurface. This implies that, once the normalization is applied, the concentration of the pigment is not relevant in discriminating the samples. This is convenient as an ideal technique should indeed be able to predict characteristic penetration depth of agent into the medium irrespective of its initial amount and concentration.

In Fig. 6, the slope value of sample 1E is also reported (concentration profile type 2). Despite sample 1E having the same penetration depth as 1C and 1D, it is grouped together instead with samples 1A and 1B. What is different for this sample (1E) from the rest is its concentration profile, and this result indicates that the concentration profile plays a significant role on the slope. Sample 1E sheds light on the need to consider both penetration depth and concentration profile as major factors that influence the micro-SORS curve slope. This confounding factor makes the interpretation of the micro-SORS data more challenging. From this one would conclude that the prediction of penetration depth is potentially possible based on a prior calibration measurement and subject to the diffusion agent, concentration profile type (*e.g.* one step or two steps of different concentration) and the matrix being identical in the prediction and calibration data sets [31].

3.2.2 Samples set 2

Samples set 2 is more challenging because the matrix (calcite) concentration changes along the depth. The diffusion concentration profiles of these samples are more complex also because all samples have a decreasing W/C from the top to the bottom layer, mimicking a more realistic concentration gradient

compared to the samples set 1. In Fig. 7a, the normalized ratio trends of samples set 2 are shown. Also in this case, the normalization was applied at 300 mm of defocusing to avoid the uncertainty of the first defocusing steps which are subject to larger fluctuations due to sample inhomogeneities. In Fig. 7b, the linear fitting of the curves is displayed. Similarly to the samples set 1, the ratio decay rate of the normalized trends seems to be dominantly influenced by the penetration depth of the agent: 2A and 2B have the smaller penetration depth of whewellite (152 μm and 140 μm, respectively); accordingly, their ratio decay rate is the fastest. 2D has the largest penetration depth of the agent (234 μm), and its ratio decay rate is the slowest as anticipated [29]. 2C ratio decay rate is in between the mentioned samples and this is consistent with its penetration depth of whewellite (172 μm), in between samples 2A-2B and 2D. In Fig. 8, the slopes of the linear fitting are reported. Here, given the underlying complexity of the diffusion process and present variation of the concentration profiles with depth, a more detailed discussion of the results is required. Samples 2A and 2B possess very similar penetration depths, as already mentioned. Moreover, they have the same concentration profiles (W/C is halved in the second layer of both samples), whereas the initial concentration of whewellite is different (the whewellite concentration is higher in both 2A layers). The slope of the linear fitting of these two samples is very similar, and their confidence intervals are partially overlapped. This indicates that similar penetration depth produces similar slope of the normalized linear fitting of the ratio trends, whereas different concentration does not affect this slope markedly, as was observed for the first samples set.

Samples 2C and 2D have different penetration depths and concentration profiles than samples 2A and 2B. Nonetheless, sample 2C has been prepared using the same W/C concentration of sample 2B (in both samples the W/C of the top layer is 0.46 whereas the W/C of the second layer is 0.20) and also the same bottom layer thickness, whereas sample 2D is completely different (three layers with different W/C ratios).

Therefore, the degree of change in comparison with samples 2A and 2B of the concentration profile is minor in sample 2C than in sample 2D. This is clearly visible in Fig. 8, where the sample 2C slope (absolute value) is higher, and thus closer to 2B, than that of sample 2D.

Based on these results, samples set 2 confirms the major role of the penetration depth and concentration profile on the micro-SORS curve slope.

4. CONCLUSIONS

The micro-SORS applicability to the study of diffusion processes has been demonstrated. The method is effective both in simple situations, where the matrix has constant concentration and in more complex materials, where the concentration of the matrix is altered along the profile in depth.

Micro-SORS is not dependent by the initial concentration of the agent applied to the surface; this is extremely important because this characteristics makes micro-SORS suitable for comparing materials that have a different amount of agent on the surface, a common situations in conservation yard.

However, micro-SORS is dependent on the shape of diffusion concentration profile inside matrix, since it also influences micro-SORS ratio curves. This indicates that when the shape of concentration profile is known, the thickness of the material involved in the diffusion process can be predicted using the slope of the normalized agent/matrix Raman intensity decay rate. A systematic micro-SORS study of concentration profile of the main products used in conservation treatments can be proposed for selected types of turbid substrates. In this way, at least for a number of cases, micro-SORS could be effectively used for the relative thickness prediction.

The limitation includes blind situations, when no information is available about the shape of concentration profiles (*e.g.* because it is unknown the extent of the decay process that involves the matrix)the slope values cannot provide any conclusive valid indications about the cross-compared penetration depths, and the data needs to be treated individually. However, fortuitously, often a common concentration profile shape can be assumed from the way the agent has been applied to matrix as discussed above - That is whether applied through a thin film or by placing large amount of it on surface, the former concentration profile established can be approximated by a half-Gaussian function and the latter by an error function [24].

References

1. L. Xie, J. Xu, Y. Zhang, and Y. He, in Advances in Bioenergy, ed by Y. Li, S.K. Khanal (Elsevier, 2020) **5**, p. 309.

2. Y. Yang, Y. Hong, and X. Wang, ACS Appl. Mater. Interfaces **13**, 8682 (2021).

3. M. A. Bolzinger, S. Briançon, J. Pelletier, and Y. Chevalier, Curr. Opin. Colloid Interface Sci. **17**, 156 (2012).

4. M. Kirkby, A. B. Sabri, D. J. Scurr, and G. P. Moss, Eur. J. Pharm. Biopharm. **159**, 77 (2021).

5. C. Conti, C. Colombo, G. Festa, J. Hovind, E. P. Cippo, E. Possenti, and M. Realini, J. Cult. Herit. **19**, 463 (2016).

6. M. Realini, C. Colombo, C. Conti, F. Grazzi, E. Perelli Cippo, and J. Hovind, Anal. Bioanal. Chem. **409**, 6133 (2017).

7. C. Conti, C. Colombo, D. Dellasega, M. Matteini, M. Realini, and G. Zerbi, J. Cult. Herit. **12**, 372 (2011).

8. C. Conti, C. Colombo, M. Matteini, M. Realini, and G. Zerbi, J. Raman Spectrosc. **41**, 1254 (2010).

9. C. Conti, I. Aliatis, C. Colombo, M. Greco, E. Possenti, M. Realini, C. Castiglioni, and G. Zerbi, J. Raman Spectrosc. **43**, 1604 (2012).

10. R. Přikryl, J. Přikrylová, M. Racek, Z. Weishauptová, and K. Kreislová, Environ. Earth Sci. **76**, 290 (2017).

11. T. Cheewaket, C. Jaturapitakkul, and W. Chalee, Constr. Build. Mater. **37**, 693 (2012).

12. Y. Jia, G. Sciutto, R. Mazzeo, C. Samorì, M. L. Focarete, S. Prati, and C. Gualandi, ACS Appl. Mater. Interfaces **12**, 39620 (2020).

13. P. M. Carmona-Quiroga, S. Martínez-Ramírez, S. Sánchez-Cortés, M. Oujja, M. Castillejo, and M. T. Blanco-Varela, J. Cult. Herit. **11**, 297 (2010).

14. F. Casadio and L. Toniolo, J. Am. Inst. Conserv. **43**, 3 (2004).

15. G. Graziani, E. Sassoni, G. W. Scherer, and E. Franzoni, Constr. Build. Mater. **148**, 571 (2017).

16. F. Hameed, B. Schillinger, A. Rohatsch, M. Zawisky, and H. Rauch, Nucl. Instruments Methods Phys. Res. Sect. A Accel. Spectrometers, Detect. Assoc. Equip. **605**, 150 (2009).

17. M. Slavíková, F. Krejčí, J. Žemlička, M. Pech, P. Kotlík, and J. Jakůbek, J. Cult. Herit. **13**, 357 (2012).

18. A. Botteon, J. Yiming, S. Prati, G. Sciutto, M. Realini, C. Colombo, and C. Castiglioni, Talanta **218**, 121078 (2020).

19. C. Conti, C. Colombo, M. Realini, G. Zerbi, and P. Matousek, Appl. Spectrosc. **68**, 686 (2014).

20. S. Mosca, C. Conti, N. Stone, and P. Matousek, Nat. Rev. Methods Prim. **1**, 22 (2021).

21. P. Matousek, M. D. Morris, N. Everall, I. P. Clark, M. Towrie, E. Draper, A. Goodship, and A. W. Parker, Appl. Spectrosc. **59**, 1485 (2005).

22. C. Conti, M. Realini, C. Colombo, A. Botteon, and P. Matousek, J. Raman Spectrosc. **47**, 565 (2016).

23. C. Conti, M. Realini, C. Colombo, and P. Matousek, Analyst **140**, 8127 (2015).

24. H. Mehrer, Diffusion in Solids, 1st edn. (Springer, Berlin, Heidelberg, 2007) pp. 37-53.

25. J. Crank, The Mathematics of Diffusion, 2nd edn. (Clarnedon Press, Oxford, 1975) pp. 13-17

26. T. Luping and J. Gulikers, Cem. Concr. Res. **37**, 589 (2007).

27. M. Matteini, Conserv. Sci. Cult. Herit. **8**, 13 (2008).

28. I. Osticioli, G. Botticelli, P. Matteini, S. Siano, R. Pini, and M. Matteini, J. Raman Spectrosc. **48**, 966 (2017).

29. S. Mosca, P. Dey, M. Salimi, B. Gardner, F. Palombo, N. Stone, and P. Matousek, Spatially Offset Raman Spectroscopy - How Deep? Anal. Chem. **Submitted**, (2021).

30. C. Conti, A. Botteon, C. Colombo, M. Realini, and P. Matousek, Anal. Chem. **89**, 11476 (2017).

31. S. Mosca, P. Dey, M. Salimi, B. Gardner, F. Palombo, N. Stone, and P. Matousek, Anal. Chem. **93**, 3386 (2021).

Figures

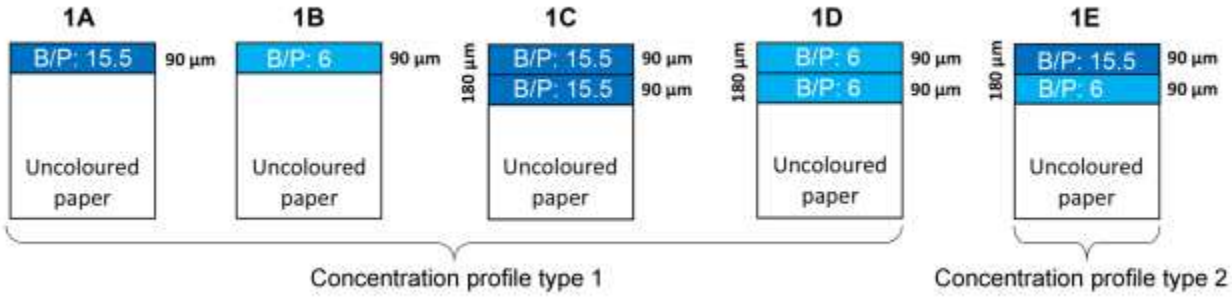

Fig. 1 Samples set 1, cross-section view. Phthalocyanine blue (B) and paper (P) ratios, concentration profile type and layers thickness are reported.

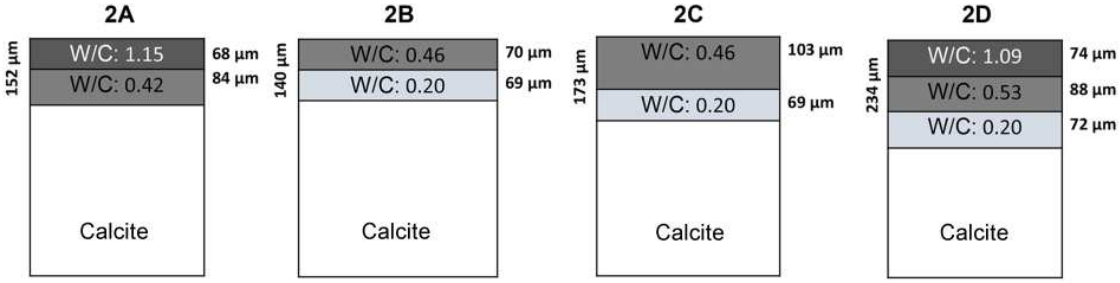

Fig.2 Samples set 2, cross-section view. Whewellite (W) and Calcite (C) ratios and layers thickness are reported

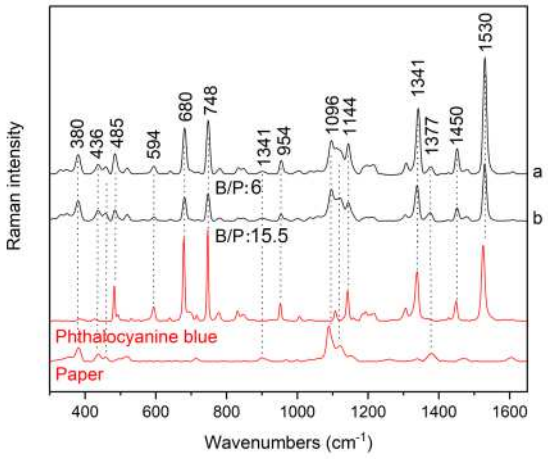

Fig.3 Representative conventional Raman spectra collected on the surface of the more intense blue (i) and the less intense blue paper sheets (ii). The reference spectra of phthalocyanine blue and paper are shown in red

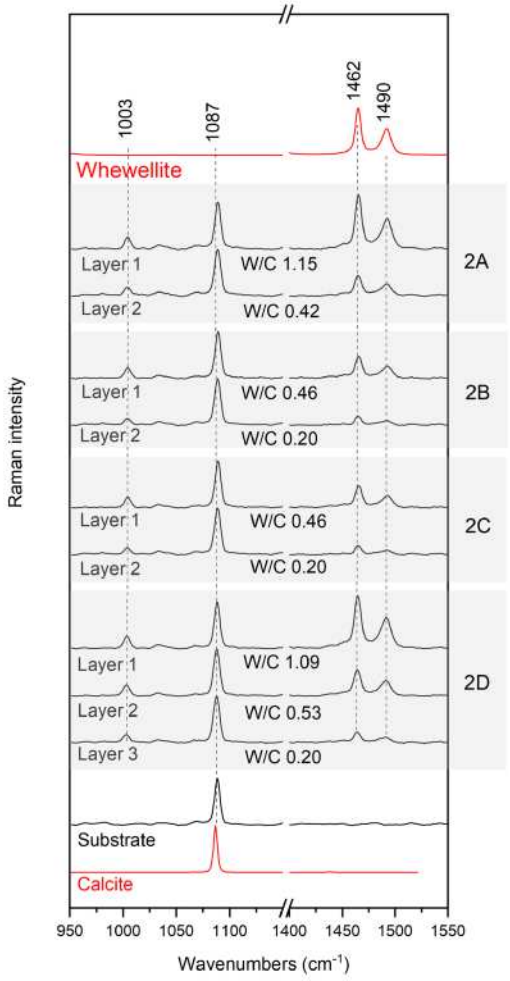

Fig.4 Representative conventional Raman spectra collected on individual layers on their cross-sections of samples set 2; reference spectrum of the calcite-based substrate is also shown. The reference spectra of whewellite and calcite are also reported in red

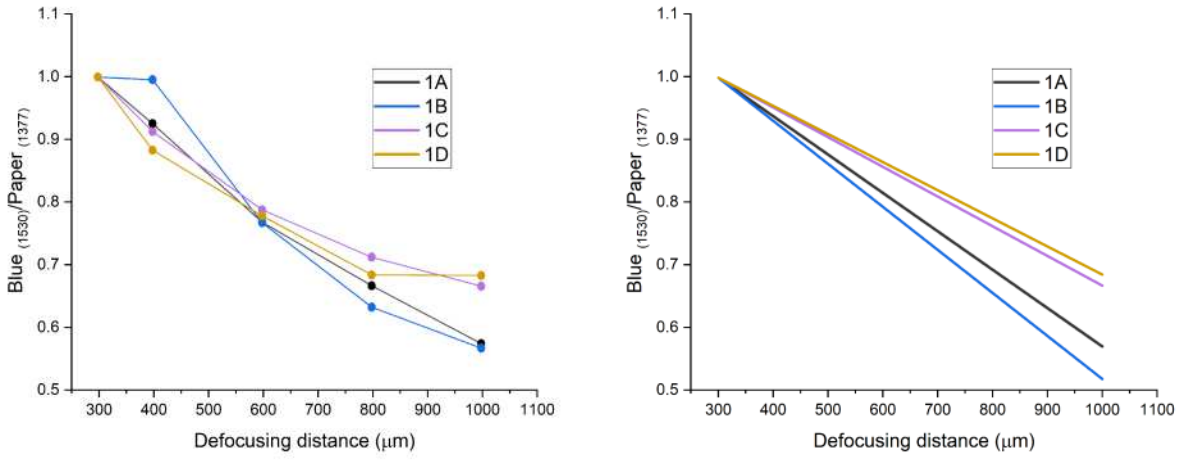

Fig.5 Normalized ratio plot (a) and linear fitting of the normalized ratio trend (b) of samples having the concentration profile type 1 (1A-1D)

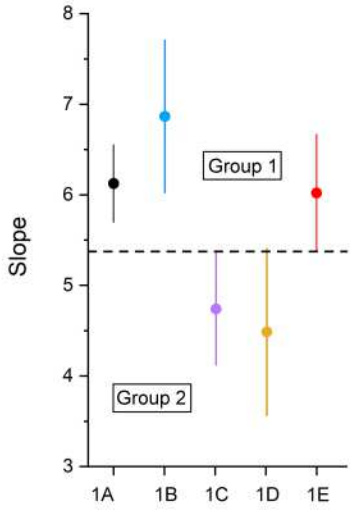

Fig.6 Slopes (absolute values) with confidence interval of the linear fitting shown in Fig. 6b. Samples 1A-1D (concentration profile type 1) can be divided in two groups basing on the slope of their ratio trends. Sample 1E (concentration profile type 2) belongs to group 1 despite its penetration depth being the same of the group 2 samples

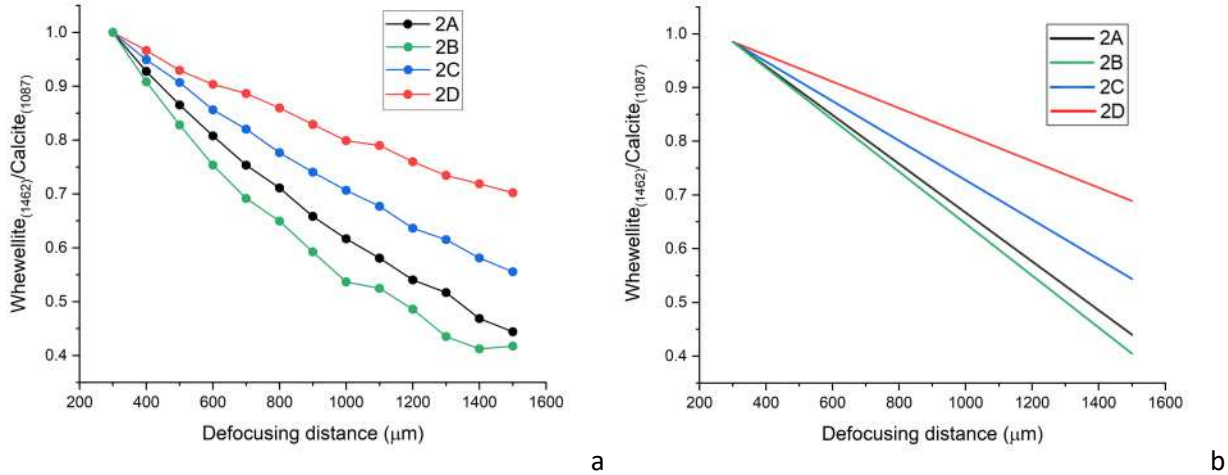

Fig.7 Normalized ratio plot (a) and linear fitting of the normalized ratio trend (b) of the second samples set

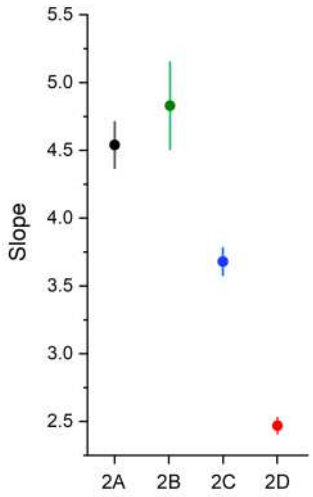

Fig.8 Slopes (absolute values) with confidence interval of the linear fitting shown in Fig. 7b